Mon. Not. R. Astron. Soc. **000**, 000–000 (2001)

Magnetorotational Instability in a Rotating Liquid Metal Annulus

Hantao Ji,[1⋆] Jeremy Goodman[2] and Akira Kageyama[1,3]
[1] *Princeton Plasma Physics Laboratory, Princeton, NJ 08543, USA*
[2] *Princeton University Observatory, Princeton, NJ 08544, USA*
[3] *National Institute for Fusion Science, Toki, Gifu 509-5292, Japan*

20 March 2001

ABSTRACT
Although the magnetorotational instability (MRI) has been widely accepted as a powerful accretion mechanism in magnetized accretion disks, it has not been realized in the laboratory. The possibility of studying MRI in a rotating liquid-metal annulus (Couette flow) is explored by local and global stability analysis and magnetohydrodynamic (MHD) simulations. Stability diagrams are drawn in dimensionless parameters, and also in terms of the angular velocities at the inner and outer cylinders. It is shown that MRI can be triggered in a moderately rapidly rotating table-top apparatus, using easy-to-handle metals such as gallium. Practical issues of this proposed experiment are discussed.

Key words: accretion: accretion disks – galaxy: disk – stars: planetary systems: protoplanetary disks

1 INTRODUCTION

Astrophysical magnetic fields have long been recognized to be important but difficult to understand. A prominent example concerns accretion disks (Shakura & Sunyaev 1973; Lynden-Bell & Pringle 1974), where orbiting plasmas gradually accrete onto a central mass. Three types of central object occur: protostars (stars in formation), collapsed stars in binary systems (white dwarfs, neutron stars, and black holes), and supermassive black holes in active galactic nuclei (quasars *et al.*). In addition to the accretion process, jets and other spectacular phenomena may be magnetically driven by the disk (e.g. Meier, Koide, & Uchida 2001). Understanding the dynamics and dissipation mechanisms in accretion disks holds an important key to understanding many active astronomical systems as a whole.

The accretion rates cannot be due to ordinary molecular or plasma viscosity because of the extraordinarily high Reynolds numbers involved. Theorists have often appealed to hydrodynamic turbulence (Pringle 1981), but recent numerical simulations indicate that nonmagnetic disks are stabilized by their positive angular momentum gradient (Balbus, Hawley, & Stone 1996; Cabot 1996; Hawley, Balbus, & Winters 1999); in effect, Rayleigh's stability criterion appears to suppress local nonaxisymmetric as well as axisymmetric disturbances (Rayleigh 1916). Linear axisymmetric instability of a *magnetized* but Rayleigh-stable fluid, the magnetorotational instability (MRI), was discovered decades ago (Velikhov 1959; Chandrasekhar 1960) but did not come to the attention of the astrophyisical community until recently rediscovered (Balbus & Hawley 1991a), despite general recognition that magnetic effects might somehow be important (Shakura & Sunyaev 1973). Since then, many analytic and numerical studies of the MRI have been performed under increasingly complex and realistic assumptions, including such effects as finite resistivity, global boundary conditions, and nonlinearity in two and three dimensions (Balbus & Hawley 1991b; Curry, Pudritz, & Sutherland 1994; Blaes & Balbus 1994; Brandenburg et al. 1995; Matsumoto & Tajima 1995; Hawley, Gammie, & Balbus 1996; Stone et al. 1996; Gammie 1996; Jin 1996; Sano & Miyama 1999; Fleming, Stone, & Hawley 2000; Hawley 2000).

Despite its popularity and importance, however, the MRI has never been realized in the laboratory or demonstrated observationally. Laboratory plasma experiments are primarily magnetically driven, and the observed flows, often induced as secondary effects of other instabilities, are small compared to the Alfvén speed. On the other hand, the existing body of experimental work on magnetized Couette flow using liquid metals (Donnelly & Ozima 1960; Donnelly & Ozima 1962; Donnelly & Caldwell 1964; Brahme 1970) has focused on magnetic stabilization of the Rayleigh instability, as first analyzed by Chandrasekhar (1961). In this Letter, we explore the feasibility of a Couette-flow experiment dedicated to MRI.

⋆ E-mail: hji@pppl.gov

2 LOCAL STABILITY ANALYSIS

Couette flow involves a liquid confined between rotating coaxial cylinders (Couette 1890). Let their radii be $r_1 < r_2$, and their angular velocities Ω_1, Ω_2. In steady state, the radial angular momentum flux, $h\cdot 2\pi r\cdot\rho\nu\cdot r^2(-\partial\Omega/\partial r)$, is constant with radius, where h is the depth of the liquid, ρ is its density, and ν is its kinematic viscosity. If $\partial h/\partial r = 0$, then the angular velocity of the liquid satisfies $r^3\partial\Omega/\partial r =$const., so that

$$\Omega(r) = a + \frac{b}{r^2}, \tag{1}$$

where $a = (\Omega_2 r_2^2 - \Omega_1 r_1^2)/(r_2^2 - r_1^2)$ and $b = r_1^2 r_2^2(\Omega_1 - \Omega_2)/(r_2^2 - r_1^2)$. The Rayleigh stability criterion is $a\Omega > 0$.

The dynamics of liquid metals is well described by the incompressible and dissipative MHD equations,

$$\begin{aligned}
0 &= \boldsymbol{\nabla\cdot V}\\
0 &= \boldsymbol{\nabla\cdot B}\\
\frac{\partial \boldsymbol{B}}{\partial t} &= \boldsymbol{\nabla\times(V\times B)} + \eta\boldsymbol{\nabla}^2\boldsymbol{B}\\
\frac{\partial \boldsymbol{V}}{\partial t} + (\boldsymbol{V}\cdot\boldsymbol{\nabla})\boldsymbol{V} &= \frac{(\boldsymbol{B}\cdot\boldsymbol{\nabla})\boldsymbol{B}}{\mu_0\rho} - \frac{1}{\rho}\boldsymbol{\nabla}\left(p + \frac{B^2}{2\mu_0}\right)\\
&\quad +\nu\boldsymbol{\nabla}^2\boldsymbol{V},
\end{aligned}$$

where $\boldsymbol{V}$ is velocity, $\boldsymbol{B}$ is magnetic field, η is magnetic diffusivity, and p is a scalar potential incorporating both pressure and gravity. In cylindrical coordinates, the equilibrium quantities are $\boldsymbol{B}_0 = (0, 0, B)$ and $\boldsymbol{V}_0 = (0, r\Omega, 0)$, and the balance of forces is $\partial p_0/\partial z = 0$ and $\partial p_0/\partial r = \rho r\Omega^2$.

WKBJ methods describe the stability of this system very well even on the largest scales. Using cylindrical coordinates, the perturbations are $\boldsymbol{B}_1 = (B_r, B_\theta, B_z)$ and $\boldsymbol{V}_1 = (V_r, V_\theta, V_z)$, all proportional to $\exp(\gamma t - ik_z z - ik_r r)$, so that γ is the growth rate and the perturbations are axisymmetric. The minimum k_z and k_r are assumed to be π/h and $\pi/(r_2 - r_1)$, respectively, so that the total wavenumber $k = \sqrt{k_z^2 + k_r^2} = k_z\sqrt{1+\epsilon^2}$, where $\epsilon \equiv h/(r_2 - r_1)$ is the elongation of a toroidal cross-section of the liquid metal annulus. The linearized equations of motion are

$$\begin{aligned}
0 &= k_r V_r + k_z V_z\\
0 &= k_r B_r + k_z B_z\\
\gamma B_r &= -ik_z B V_r - \eta k^2 B_r\\
\gamma B_\theta &= -ik_z B V_\theta + \frac{\partial\Omega}{\partial\ln r}B_r - \eta k^2 B_\theta\\
\gamma V_r - 2\Omega V_\theta &= -i\frac{k_z B}{\mu_0\rho}B_r + i\frac{k_r}{\rho}p_1 + i\frac{k_r B}{\mu_0\rho}B_z - \nu k^2 V_r\\
\gamma V_\theta + \frac{\kappa^2}{2\Omega}V_r &= -i\frac{k_z B}{\mu_0\rho}B_\theta - \nu k^2 V_\theta\\
\gamma V_z &= i\frac{k_z}{\rho}p_1 - \nu k^2 V_z
\end{aligned}$$

where the epicyclic frequency is defined by $\kappa^2 \equiv (1/r^3)\partial(r^4\Omega^2)/\partial r = 4\Omega^2 + \partial\Omega^2/\partial\ln r$ and p_1 is the perturbed pressure. The vertical induction equation is not needed since B_z can be deduced from $\boldsymbol{\nabla\cdot B} = 0$. These equations lead to the following dispersion relation:

$$\begin{aligned}
[(\gamma+\nu k^2)(\gamma+\eta k^2) + (k_z V_A)^2]^2\frac{k^2}{k_z^2} &+ \kappa^2(\gamma+\eta k^2)^2\\
&+ \frac{\partial\Omega^2}{\partial\ln r}(k_z V_A)^2 = 0.
\end{aligned}$$

The Alfvén speed is $V_A \equiv B/\sqrt{\mu_0\rho}$. This dispersion relation is identical to the one derived for accretion disks in the incompressible limit (Sano & Miyama 1999).

Introducing a dimensionless vorticity parameter, $\zeta \equiv (1/r\Omega)\partial(r^2\Omega)/\partial r = 2 + \partial\ln\Omega/\partial\ln r$, we have $\kappa^2 = 2\Omega^2\zeta$ so that the Rayleigh stability criterion becomes $\zeta \geq 0$. Similarly, $\partial\Omega^2/\partial\ln r = 2\Omega^2(\zeta - 2)$. There are three other relevant frequencies: resistive, $\omega_\eta \equiv \eta k^2$; viscous, $\omega_\nu \equiv \nu k^2$; and Alfvénic $\omega_A \equiv |k_z V_A|$. Because liquid metals are far more resistive than viscous, ω_η serves as a base frequency in the following three dimensionless parameters: magnetic Prandtl number, $P_{\rm m} \equiv \omega_\nu/\omega_\eta$; Lundquist number, $S \equiv \omega_A/\omega_\eta$; and magnetic Reynolds number, $R_{\rm m} \equiv \Omega/\omega_\eta$. The astrophysical literature gives several inequivalent definitions of "magnetic Reynolds number," some corresponding to our S. Some involve the sound speed, c_s, for although MRI is essentially noncompressive, vertical force balance in an astrophysical disk relates c_s to the half-thickness: $c_s \approx h\Omega$. The free energy for MRI derives from differential rotation, represented in our dimensionless system by a combination of ζ and $R_{\rm m}$; but magnetic field, represented by S, is required to liberate this energy from hydrodynamic constraints.

Using the normalized growth rate, $\gamma/\omega_\eta \to \gamma$, the dispersion relation is rewritten as

$$\begin{aligned}
\left[(\gamma+P_m)(\gamma+1)+S^2\right]^2(1+\epsilon^2) &+ 2\zeta R_m^2(\gamma+1)^2\\
&- 2(2-\zeta)R_m^2 S^2 = 0.
\end{aligned}$$

The necessary and sufficient condition for stability is

$$(P_{\rm m}+S^2)^2(1+\epsilon^2) + 2\zeta R_{\rm m}^2 - 2(2-\zeta)R_{\rm m}^2 S^2 \geq 0, \tag{2}$$

which can be taken into various limits.

Nonmagnetic limit. As $\eta \to \infty$, the three terms S^4, $R_{\rm m}S^2$, and $R_{\rm m}^2 S^2$ approach zero faster than the others, leading to the stability condition $P_{\rm m}^2(1+\epsilon^2) + 2\zeta R_m^2 \geq 0$. Stability occurs when $\zeta \geq 0$, and also when $\zeta < 0$ if the Taylor number $-2\zeta\Omega^2/\nu^2 k^4 \leq 1 + \epsilon^2$ (Taylor 1923).

Ideal MHD limit. As $\eta \to 0$, the other two terms dominate, with stability for $S^2(1+\epsilon^2) \geq 2(2-\zeta)R_{\rm m}^2$. Instability occurs at sufficiently weak fields (small S) unless $\zeta \geq 2$, *i.e.* $\partial\ln\Omega/\partial\ln r \geq 0$ (Balbus & Hawley 1991a).

Small $P_{\rm m}$ limit. In liquid metals, usually viscosity is much smaller than resistivity, $P_{\rm m} \sim 10^{-6}$. As $P_{\rm m} \to 0$, eq. (2) reduces to

$$\zeta \geq \frac{2S^2}{S^2+1} - \frac{S^4(1+\epsilon^2)}{2R_{\rm m}^2(S^2+1)}\,. \tag{3}$$

3 STABILITY DIAGRAMS AND GROWTH RATES

The stability condition (3) defines a two-dimensional surface in the parameter space $(S, \zeta, R_{\rm m})$ at fixed ϵ. To illustrate the dependence on these parameters, we vary only two of them at a time. Stability boundaries in the (S, ζ) plane are shown in Fig. 1. When $\zeta < 0$, the annulus is unstable hydrodynamically to the Rayleigh mode at $S = 0$ but can be stabilized (Chandrasekhar 1961) by a large magnetic field (large S). When $\zeta > 0$, the annulus is stable at zero field but unstable

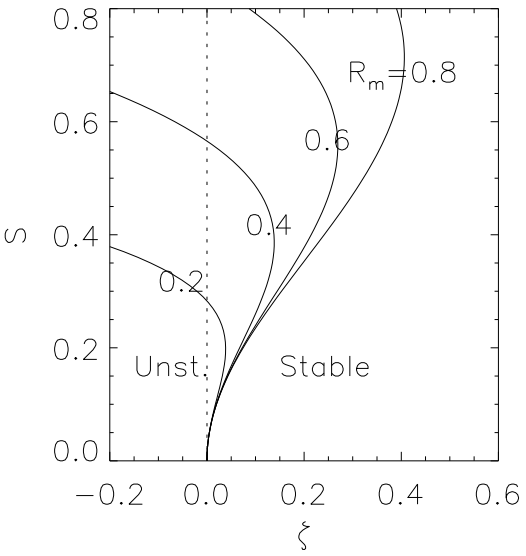

Figure 1. Stability of a rotating liquid metal annulus in dimensionless parameter space of (S, ζ) at a few values of $R_{\rm m}$. Areas to right of the curves indicate stability.

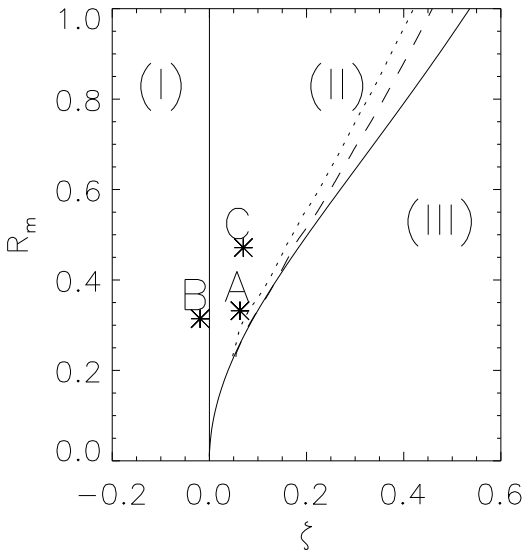

Figure 2. Stability of a rotating liquid metal annulus in $R_{\rm m}$ and ζ space. Here the stability can be divided into 3 regions: region (I) is hydrodynamically unstable but can be stabilized by a finite magnetic field, as exemplified by point B. Region (II) is hydrodynamically stable but can be destabilized by presence of a magnetic field (MRI), as exemplified by points A and C. Region (III) is always stable. Results from global eigenmode analysis are also shown: dotted lines for conducting boundary conditions and dashed lines for insulating boundary conditions.

at some $S > 0$ if $R_{\rm m}$ is large enough. Stability returns at even larger S. The unstable region extends to larger S and ζ at larger $R_{\rm m}$. Stability at $S = 0$ and as $S \to \infty$ are hallmarks of MRI (Balbus & Hawley 1991a; Balbus & Hawley 1998). (In ideal MHD, instability extends formally to $S = 0^+$.) It can be seen that there is a maximum ζ above which MRI is absent for a given $R_{\rm m}$. From eq.(3),

$$\zeta_{\rm max} = 2 - \frac{1+\epsilon^2}{R_m^2}\left(\sqrt{1+\frac{4R_m^2}{1+\epsilon^2}} - 1\right) \qquad (4)$$

at the S value given by $S^2 = \sqrt{1 + 4R_m^2/(1+\epsilon^2)} - 1$.

Figure 2 shows stability in the $(R_{\rm m}, \zeta)$ plane. Region (I) is hydrodynamically unstable but can be stabilized by a finite magnetic field. This region has been extensively studied both theoretically and experimentally (Chandrasekhar 1961), and is exemplified by point B. Region (II) is hydrodynamically stable but destabilized by a magnetic field. This is the MRI region, and has never been studied experimentally. Growth rates at points A and C are given below. Region (III) is always stable. The boundary between regions (II) and (III) is given by eq. (4).

It is useful to project the stability diagram onto experimentally controllable parameters. To apply the local dispersion relation, we take $\zeta = 2a/\bar{\Omega}$ [from eq.(1)] and $R_{\rm m} \equiv \bar{\Omega}/\omega_\eta$, with $\bar{\Omega} \equiv \sqrt{\Omega_1\Omega_2}$. Figure 3(a) shows stability in the plane (Ω_1, Ω_2) for an annulus of dimensions r_1=0.05m, r_2=0.15m, and h=0.1m (hence $\epsilon = 1$) filled with gallium. Table 1 lists the physical parameters at points A, B, and C. The corresponding growth rates are shown as functions of magnetic field in Fig.3(b).

The applicability of WKBJ is subject to doubt, since the most unstable wavelengths are larger than the gap width and cylinder height. In fact, global analysis shows that the eigenfunctions are nonsinusoidal and sensitive to the boundary conditions. Yet the growth rates are remarkably robust. A linearized, finite-difference, initial-value code was written to to detect the fastest growing mode. Periodic boundary conditions were used in z. Radial boundaries were impenetrable and no-slip ($\delta \boldsymbol{V}_1 = 0$), and electrically either perfectly insulating or perfectly conducting. Results are compared with the WKBJ analysis in Figs.2 and 3. Figure 4 shows eigenmodes for the parameters of point C with B=0.3 Tesla. Differences between the conducting and insulating cases can be seen near the inner boundaries. Nevertheless, the growth rates are remarkably similar to those of the local analysis, which therefore should suffice for preliminary experimental design. [Details of the global analysis will be reported elsewhere (Goodman & Ji 2001).]

Table 1. Parameters for a gallium annulus with $r_1 = 0.05$m, $r_2 = 0.15$m, and $h = 0.1$m.

point	Ω_1(rpm)	Ω_2(rpm)	R_m	ζ
A	3600.00	435.00	0.3319	0.06293
B	3600.00	390.00	0.3143	-0.01899
C	5089.77	620.70	0.4715	0.06984

A fully nonlinear incompressible MHD code has been developed to study the problem in three dimensions (Kageyama, Ji, & Goodman 2001). Initial results ¿from linear and two-dimensional runs of this code with conducting, freely-slipping boundary conditions agree with the local and global analyses. For example, for the conditions given by the point C in Figs.2 and 3 at $B = 0.3$ Tesla, the growth rate is 21.67 $\rm s^{-1}$ from simulations, 21.90 $\rm s^{-1}$ from global analysis, and 19.10 $\rm s^{-1}$ from local analysis.

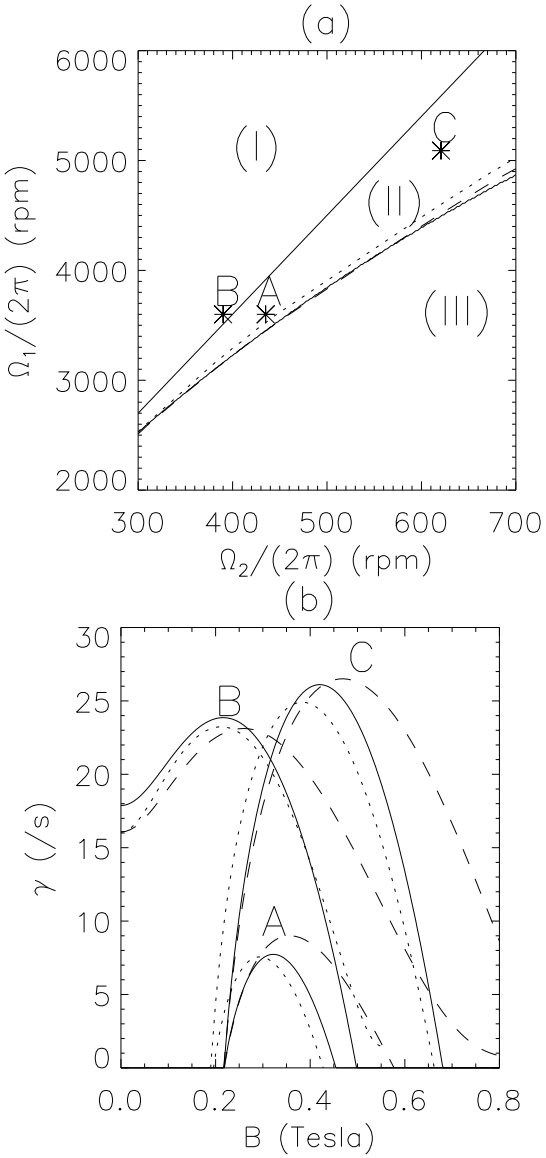

Figure 3. Stability diagram of a rotating gallium annulus in Ω_1 and Ω_2 space with dimensions r_1=0.05m, r_2=0.15m, and h =0.1m. The growth rates of points A, B, and C, corresponding to those in Fig.2, are also shown as functions of magnetic field in (b). Results from global eigenmode analysis are also shown: dotted lines for conducting boundary conditions and dashed lines for insulating boundary conditions.

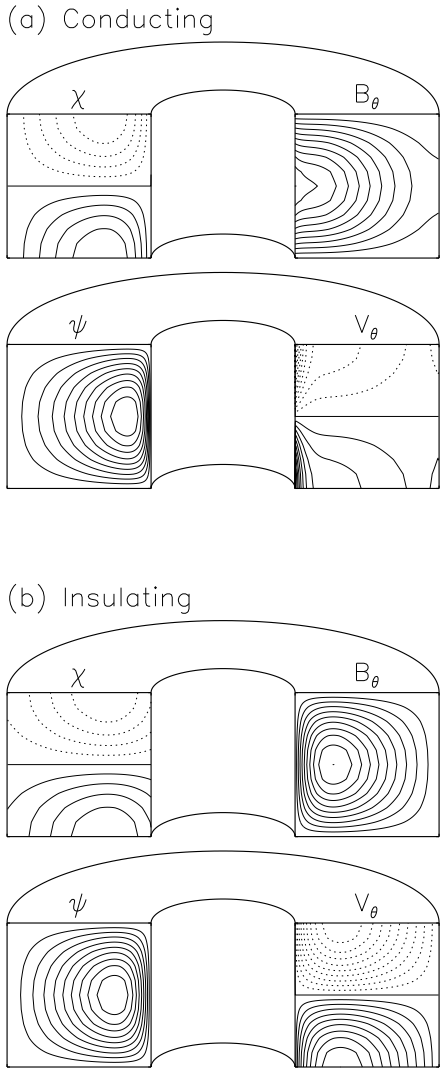

Figure 4. Eigenmodes for conditions given by point C in Fig.3 at $B = 0.3$ Tesla with conducting (a) and insulating (b) radial boundaries. Here, solid (dotted) lines represent positive (negative) values; χ and ψ are poloidal flux and stream functions, respectively.

4 DISCUSSIONS AND CONCLUSIONS

Several issues must be explored before committing to an experimental design. The first is geometric optimization with regard to aspect ratio [$A \equiv (r_2 + r_1)/(r_2 - r_1)$] and elongation [$\epsilon \equiv h/(r_2 - r_1)$]. Obviously, $\epsilon \sim 1$ is desirable to minimize volume, and therefore expense, at a given growth rate. Less obviously, aspect ratios close to unity cause the eigenmodes and growth rates to be dominated by the inner cylinder, which is undesirable if the aim is to imitate relatively uniform local conditions within an astrophysical disk. Therefore, moderate values of $A(\sim 2)$ and $\epsilon(\sim 1)$ are preferred.

The periodic vertical boundary conditions used in all of our analyses take no account of viscous layers at the top

and bottom of the flow. (The top will have to be capped because of large radial pressure gradients.) The main effect of these viscous boundary layers is to drive Ekman circulation, which flows more rapidly against a weak angular-momentum gradient than against uniform rotation. The thickness of the Ekman layer $\delta_E \approx \zeta^{-1/4}\sqrt{\nu/\bar{\Omega}}$ is small ($\sim 10^{-3}\,h$ at point C), and the Ekman circulation time $\zeta^{3/4}h/\sqrt{\nu\bar{\Omega}} \sim 2$ s is much longer than a typical MRI growth time, so we do not expect these layers to be important for stability. To further minimize their effect, if necessary, one could increase ϵ, use differentially rotating rings at the vertical boundaries, or modify the boundary layer by localized Lorentz forces (Brahme 1970).

A third issue is finite-amplitude or nonlinear hydrodynamical instability in Rayleigh-stable regimes. Few theoretical studies on this subject exist (Serrin 1959; Joseph & Munson 1970). It has been argued from experiments that a rapid Couette flow can be nonlinearly unstable (Richard & Zahn 1999). However, there are indications that such instabilities are caused by wall surface defects (Schultz-Grunow 1959), which can be minimized. In fact, it has been shown numerically that a positive angular-momentum gradient strongly resists nonlinear instability (Balbus, Hawley, & Stone 1996; Hawley, Balbus, & Winters 1999). The outcome depends, however, on the amplitude of the initial perturbation and the strength of the angular-momentum gradient. These questions could be addressed empirically and relatively inexpensively in prototype experiments using water.

One would like to predict the nonlinear phases of MRI in the laboratory system. Ultimately, nonlinear MRI is closely related to other important physics of accretion disks involving magnetic field, i.e., dynamo processes and jet formation. Ongoing three-dimensional MHD simulations (Kageyama, Ji, & Goodman 2001) will provide useful insights here. Indeed, an important purpose of the experiment is to be a testbed for MHD codes since, lacking detailed observational constraints, theorists depend upon computer simulations to understand MRI-driven turbulence.

The experiment will be far more resistive than most accretion disks, though perhaps not all (Gammie 1996; Gammie & Menou 1998). Simulations indicate that when the field is generated by the disk itself (magnetic dynamo), then the large-scale field is nearly toroidal, the important instabilities are nonaxisymmetric, and the turbulence sustains itself only if S and $R_{\rm m}$ are much larger than the experiment proposed here will achieve (Balbus & Hawley 1991b; Brandenburg et al. 1995; Hawley, Gammie, & Balbus 1996; Sano, Inutsuku & Miyama 1998; Fleming, Stone, & Hawley 2000). On the other hand, the innermost (and therefore most energetic) parts of accretion disks often encounter a vertical field due to the central compact object. The works cited above find that in the presence of an imposed vertical field, turbulence is driven by axisymmetric modes and persists to higher resistivity, probably into the experimentally accessible regime.

In summary, we have used linear stability analyses and MHD simulations to explore the prospects for magnetorotational instability in a magnetized Couette flow. We find that MRI can be achieved in a moderately rapidly rotating table-top apparatus using an easy-to-handle liquid metal such as gallium. Auxiliary experiments with an inexpensive nonmagnetic fluid, such as water, will be valuable both as prototypes and as controls to distinguish MRI from nonlinear hydrodynamic instabilities. Onset and dynamics of MRI can be detected by torque measurements of cylinders and magnetic sensors placed around the annulus. Ultrasonic imaging may also be possible. If successful, this will be a rare example of an astrophysical process that can be studied in the laboratory.

Acknowledgments

The authors are grateful to Drs. P. Diamond, R. Goldston, S. Hsu, R. Kulsrud, W. Tang, and M. Yamada for fruitful discussions. This work is supported by U.S. Department of Energy and by NASA grant NAG5-8385 [to JG].

REFERENCES

Balbus, S.A., Hawley, J.F. 1991, ApJ, 376, 214
Balbus, S.A., Hawley, J.F. 1991, ApJ, 376, 223
Balbus, S.A., Hawley, J.F. 1998, Rev. Mod. Phys., 70, 1
Balbus, S.A., Hawley, J.F., Stone, J.M. 1996, ApJ, 467, 76
Blaes, O.M., Balbus, S.A. 1994, ApJ, 421, 163
Brandenburg, A., Nordlund, Å., Stein, R.F., Torkelsson, U. 1995, ApJ, 446, 741
Brahme, A. 1970, Physica Scripta, 2, 108
Cabot, W. 1996, ApJ, 465, 874
Chandrasekhar, S. 1960, Proc. Nat. Acad. Sci., 46, 253
Chandrasekhar, S. 1961, Hydrodynamic and Hydromagnetic Stability, London: Oxford University Press
Couette, T. 1890, Ann. Chim. Phys., 21, 433
Curry, C., Pudritz, R.E., Sutherland, P.G. 1994, ApJ, 434, 206
Donnelly, R. J. Caldwell, D. R. 1964, J. Fluid Mech., 19, 257
Donnelly, R. J. Ozima, M. 1960, Phys. Rev. Lett., 4, 497
Donnelly, R. J. Ozima, M. 1962, Proc. R. Soc. Lond. A, 266, 272
Fleming, T.P., Stone, J.M., Hawley, J.F. 2000, ApJ, 530, 464
Gammie, C.F. 1996, ApJ, 457, 355
Gammie, C.F. & Menou, K. 1998, ApJ, 492, L75
Goodman, J., Ji, H. 2001, to be submitted
Hawley, J.F. 2000, ApJ, 528, 462
Hawley, J.F., Balbus, S.A., Winters, W.F. 1999, ApJ, 518, 394
Hawley, J.F., Gammie, C.F., Balbus, S.A. 1996, ApJ, 464, 690
Jin, L. 1996, ApJ, 457, 798
Joseph, D.D., Munson, B.R. 1970, J. Fluid Mech., 43, 545
Kageyama, A., Ji, H., Goodman, J. 2001, to be submitted
Lynden-Bell, D., Pringle, J.E. 1974, MNRAS, 168, 603
Matsumoto, R., Tajima, T. 1995, ApJ, 445, 767
Meier, D.L., Koide, S., Uchida, Y. 2001, Sci, 291, 84
Pringle, J.E. 1981, ARA&A, 19, 137
Richard, S., Zahn, J.P. 1999, A&A, 347, 734
Rayleigh, L. 1916, Proc. R. Soc. Lond. A, 93, 148
Sano, T., Inutsuku, S., & Miyama, S. 1998, ApJ, 506, L57
Sano, T., Miyama, S. 1999, ApJ, 515, 776
Schultz-Grunow, F. 1956, Z. angew. Math. Mech., 39, 101
Serrin, J. 1959, Arch. Ration. Mech. Anal., 3, 1
Shakura, N.I., Sunyaev, R.A. 1973, A&A, 24, 337
Stone, J.M., Hawley, J.F., Gammie, C.F., Balbus, S.A. 1996, ApJ, 463, 656
Taylor G.I. 1923, Phil. Trans. Roy. Soc. London A, 223, 289
Velikhov, E.P. 1959, Sov. Phys. JETP 36, 995